

Research Report

**FRONTO-PARIETAL CONNECTION ASYMMETRY
REGULATES WORKING MEMORY DISTRACTIBILITY**

FREDRIK EDIN

*School of Computer Science and Communication
Kungliga Tekniska Högskolan
SE-100 44 Stockholm, Sweden
Pediatric Neurology Research Unit
Department of Woman and Child Health, MR Center N:8
Karolinska Institutet, SE-171 76 Stockholm, Sweden
Fredrik.Edin@ki.se
<http://www.csc.kth.se/~freedin>*

TORKEL KLINGBERG

*Pediatric Neurology Research Unit
Department of Woman and Child Health, MR Center N:8
Karolinska Institutet, SE-171 76 Stockholm, Sweden
Torkel.Klingberg@ki.se
<http://www.klingberglab.se/people/torkel>*

TOMMY STÖDBERG

*Department of Woman and Child Health
Astrid Lindgrens Barnsjukhus, Q2:8
Karolinska Sjukhuset, SE-171 76 Stockholm, Sweden
Tommy.Stodberg@karolinska.se*

JESPER TEGNÉR

*Computational Biology, Department of Physics
Linköping University of Technology
SE-581 53 Linköping, Sweden
Computational Medicine Group, Department of Medicine
M:01, Karolinska Institutet, SE-171 76 Stockholm, Sweden
jesper@karlavagen90.se
<http://www.karlavagen90.se>*

Received 17 September 2007

Accepted 31 October 2007

Recent functional magnetic resonance imaging studies demonstrate that increased task-related neural activity in parietal and frontal cortex during development and training is positively correlated with improved visuospatial working memory (vsWM) performance. Yet, the analysis of the corresponding underlying functional reorganization of the fronto-parietal network has received little attention. Here, we perform an integrative experimental

and computational analysis to determine the effective balance between the superior frontal sulcus (SFS) and intraparietal sulcus (IPS) and their putative role(s) in protecting against distracters. To this end, we performed electroencephalographic (EEG) recordings during a vsWM task. We utilized a biophysically based computational cortical network model to analyze the effects of different neural changes in the underlying cortical networks on the directed transfer function (DTF) and spiking activity. Combining a DTF analysis of our EEG data with the DTF analysis of the computational model, a directed strong SFS \rightarrow IPS network was revealed. Such a configuration offers protection against distracters, whereas the opposite is true for strong IPS \rightarrow SFS connections. Our results therefore suggest that the previously demonstrated improvement of vsWM performance during development could be due to a shift in the control of the effective balance between the SFS–IPS networks.

Keywords: Working memory; computational neuroscience; EEG; directed transfer function; connectivity; frontal cortex; parietal cortex; neuronal circuits; cortico-cortical interactions; distractibility.

1. Introduction

Working memory (WM), the ability to maintain and manipulate goal-relevant information for several seconds, is a key cognitive function that underlies other cognitive abilities such as complex reasoning [1–4]. The importance of WM is demonstrated in several diseases of cognition, such as attention-deficit hyperactivity disorder, schizophrenia and Parkinson’s disease, where WM deficits are found [5–8].

Previous studies have shown that visuospatial WM (vsWM) relies on the activation of cortices in both the superior frontal sulcus (SFS) and the intraparietal sulcus (IPS) [9–12]. Furthermore, a strengthening of connections between these brain regions leads to stronger total connectivity in the vsWM network which in turn causes increased neural activity and improved vsWM task performance [13, 14]. In order to retain relevant information in WM, it is also necessary to ignore task irrelevant and distracting stimuli from the surroundings. The importance of inter-regional connections for vsWM function has been further demonstrated by Sakai *et al.* [15], who found that stronger correlations between IPS and SFS are related to increased resistance. However, the mechanisms and relative contributions by the IPS \rightarrow SFS and SFS \rightarrow IPS connection in improving distracter resistance are still largely unknown. These questions can be explored using the directed transfer function (DTF), a method based on autoregressive modeling of brain activity time series data that has the possibility to uncover the directionality of connections between brain regions [16–18], and that has been used to infer causal relations both from EEG data and local field potential (LFP) data [16, 19–21].

In the only study to date that has investigated bidirectional connectivity between IPS and SFS during memory maintenance, Babiloni *et al.* [16] used the DTF to obtain results suggesting that SFS–IPS connectivity is symmetric. However, the task used in their study only contained a single visual stimulus, far below the capacity limit of humans, whereas distracters typically affect performance in WM tasks when WM load is close to the capacity limit [22]. Equally important, it is not clear how differences in the biophysical properties of SFS and IPS affect the measurements

of effective connectivity. Effective connection strength is defined in terms of changes in spiking activity [23], but measurements of effective connectivity are usually made from something other than spiking activity, such as EEG activity. Since the relationship between spiking activity and EEG activity is modified by the biophysical properties of the brain regions, a direct interpretation of this data is unlikely to provide enough information regarding the inter-regional connectivity during vsWM and its relation to distracter resistance. Another unknown factor which might also affect the relationship between fronto-parietal asymmetry and distracter resistance is whether visual stimuli enter into the vsWM network via IPS along the dorsal stream [24–26] or whether they enter into both IPS and SFS [27, 28].

Considering the degree of SFS–IPS asymmetry and the entry point of visual stimuli, there are six possible configurations of the vsWM network (Fig. 1). Either the fronto-parietal connections are effectively stronger than the parieto-frontal connections (we will refer to this type of asymmetry as “fronto-parietal”), or the

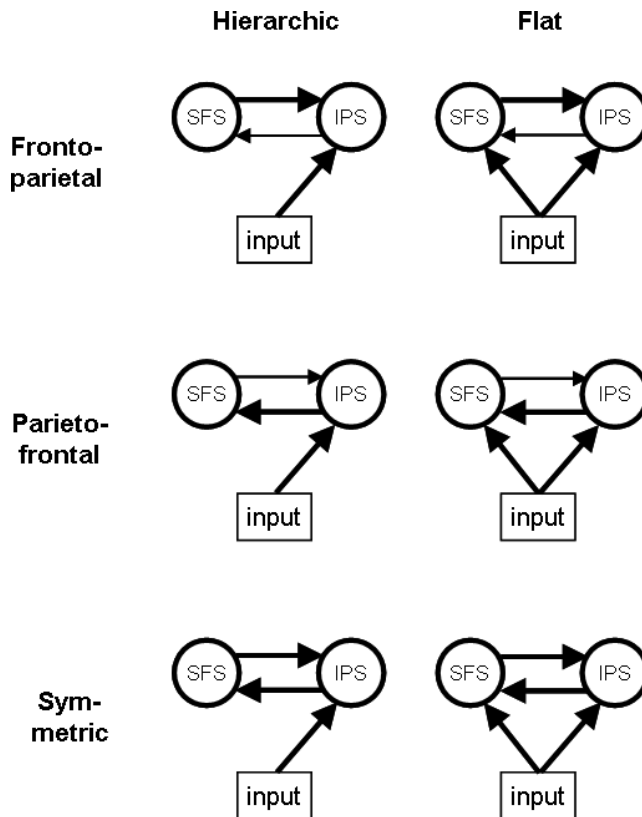


Fig. 1. Different functional configurations of the vsWM network. Rows: “Fronto-parietal”. SFS → IPS connections are more effective than IPS → SFS connections. “Parieto-frontal”. IPS → SFS connections are more effective than SFS → IPS connections. “Sym-metric”. Both connections are equally effective. Columns: “Hierarchic”. Stimuli enter IPS only, meaning that the two brain regions are at different levels of the visual processing hierarchy. “Flat”. Cue and distracter stimuli enter both regions, implying a flat organization of the two regions.

parieto-frontal connections are more effective (“parieto-frontal”), or they are equally effective (“symmetric”). In addition, visual stimuli either enter via the IPS only (we will call this route of activation “hierarchical”, since the two regions will be on different levels in the visual hierarchy [29, 30]) or via both regions (a “flat” hierarchy).

To determine the asymmetry of effective strength in the SFS–IPS connection and its functional effects on vsWM performance, access to large numbers of simultaneous frontal and parietal recordings in monkeys performing a vsWM task would be ideal. Given the absence of such data, we calculated the DTF from EEG data collected during the performance of a vsWM task during maximal memory load. To interpret the DTF, we implemented the different network configurations shown in Fig. 1 in a biophysically based computational model. This model has previously been used successfully to causally relate structural development in the child to improvements in vsWM capacity and related increases in brain activity in the SFS–IPS network [14]. With this model, we simulated DTF to relate the experimentally obtained DTF values to the underlying effective connectivity of the SFS–IPS connection. Next, to determine how visual stimuli enter the vsWM network, we compared computational model simulations from the networks in Fig. 1 to previous functional magnetic resonance imaging (fMRI) data on the processing of visual distracting stimuli during working memory maintenance [15]. In this way, we could determine which of the network configurations in Fig. 1 best mirrors the effective connectivity of the SFS–IPS working memory network. To address the functional importance of the effective connectivity between SFS and IPS, we performed computer simulations to reveal how the SFS–IPS connectivity regulates sensitivity to visual distracting stimuli.

2. Methods

2.1. *vsWM model*

The structure of the vsWM network model was the same as in Edin *et al.* [14] and is shown in Fig. 2(a) and 2(b). The network contains two interconnected regions, each consisting of a population of 128 pyramidal cells (P), and a population of 32 inhibitory interneurons (I). Every cell codes for an angle in the visual field. The two regions are replicas of the frontal region network in Tegnér *et al.* [32], and consists of Hodgkin-Huxley type cells with ion channels and input-output relations matching those of layer II/III neurons. The regions are connected only through their pyramidal cells. Connection strength was limited to assure that the absence of activity in one region would not disrupt activity in the other region [31]. Inter-regional connections have a conduction delay [33], whereas all other connections are instantaneous. There exists a topography in the connection strength between pyramidal cells within or between two regions, as indicated by the connection curve (Fig. 2(b)). The curve shows that cells with similar preferred angles are strongly connected whereas cells coding for dissimilar angles are weakly connected [34]. In simulations, connection strength was varied by varying the mean connection strength, G_{xy} . For further details of the model, see *Appendix*.

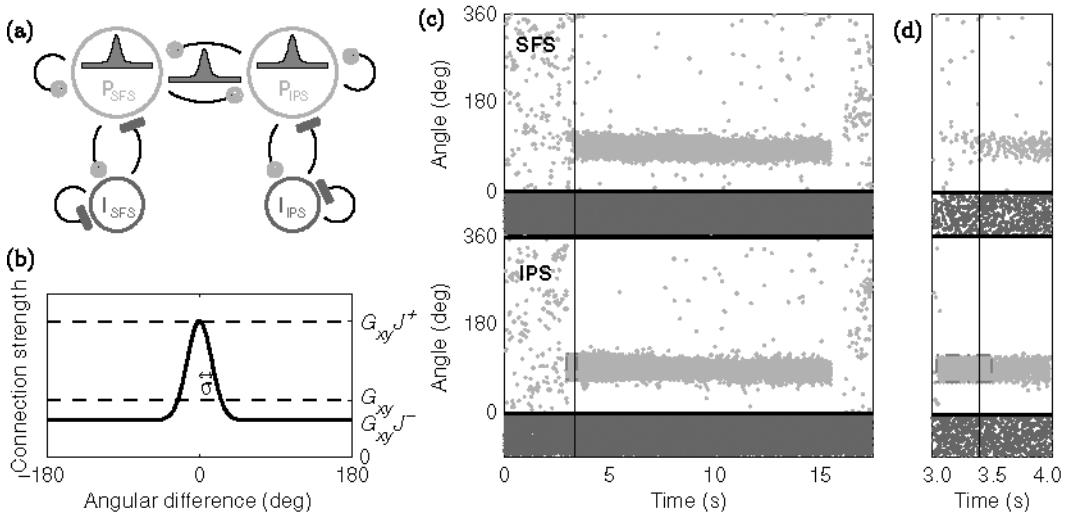


Fig. 2. The SFS-IPS vsWM network. (a) Network structure. The SFS and IPS regions both consist of a pyramidal cell population (P) and an inhibitory interneuron population (I). They are connected internally and with the other population. The Gaussian-like curves are connection curves (see b). (b) The connection curve indicates how the connection strength between two pyramidal cells within or between two regions depends on the difference in their preferred angle. In the model, the connection curve has the shape of a Gaussian curve on top of a box. G_{xy} is the mean connection strength from area y onto area x . $G_{xy}J^+$ is the height of the connection curve, and σ is the standard deviation of the Gaussian curve. To regulate the shape of the connection curve while preserving total connection strength (area under curve), changes in σ or J^+ are compensated by changes in J^- . (c) Example simulation of the vsWM trial using the “hierarchic symmetric” network in Fig. 1 with recurrent excitation only via NMDA channels. Spikes are shown as dots. Pyramidal cells are aligned along the y axis according to their preferred angles (between 0–360°). Dark grey dash-dotted square: cue. Black vertical line: lag of activation between the IPS and SFS is 320 ms. (d) Magnification to highlight the lag in activation of the frontal region.

2.2. Simulation of local field potentials

We simulated LFP from the model with 1000 Hz sampling frequency to compare with the EEG data obtained experimentally. The LFP in a small area of the brain can be approximated as a spatial average of the potential difference between distal parts of the apical dendrite and the proximal parts of the apical dendrite across pyramidal cells [35]. This is readily calculated in the model by calculating the average voltage difference between the distal and proximal apical dendritic compartments of the pyramidal cells. Since spatial smearing of the local fields by the skull does not affect DTF calculations on EEG data [16], DTF on experimental EEG data is comparable to DTF calculations on simulated LFP, except for the different frequency bands that could be attenuated to different degrees when passing through the skull. Simulated LFP data was obtained from 10 s long simulation time segments of cue, delay or baseline activity for different degrees of inter-regional connection strength asymmetry, different NMDA ratios and both symmetrical and asymmetrical stimulus presentation as described in the results subsection *The vsWM network*

has a “fronto-parietal” effective connectivity. For each set of model parameters, 12 simulations were made.

2.3. EEG recordings of vsWM-related brain activity

27 right-handed subjects with epilepsy were recruited from the epilepsy unit at Astrid Lindgren’s Children’s Hospital for WM training (not analyzed in this study), and EEG was measured during testing of performance in a vsWM task, as approved by the regional ethical vetting committee in Stockholm. The fact that the subjects had epilepsy is considered of minor importance for this study, since the epilepsy of the patients was of highly varying etiology, with half of the subjects having generalized and the other half partial epilepsy. We therefore believe that any changes in brain structure and activity due to epilepsy will not result in any systematic changes in measurements of EEG power and fronto-parietal connectivity. One subject declined and three subjects were removed because EEG sessions contained too much epileptic (two subjects) or muscle (one subject) activity. Thus, 23 subjects (13 girls and 10 boys), aged 11.6 ± 2.4 years (sample mean \pm standard deviation), remained after data preprocessing. Subjects performed two sessions of a set of cognitive tests on different days sitting in a chair ca 70 cm away from the computer screen. Each session lasted about 45 min, but EEG was only analyzed from a vsWM task (Fig. 4), which lasted about 10 min. In the task, circles were presented sequentially on a four-by-four grid. Each circle was presented for 1 s with a delay phase of 0.5 s between presentations. After all stimuli had been presented, the subject was instructed to respond by clicking in the corresponding squares in the same order as the stimuli had been presented. After three correct responses, task difficulty was increased by one item. After one erroneous trial, task difficulty was instead decreased by one. Before testing, the subjects were allowed to practice the task for 2–3 min. The average difficulty level for the recorded trials was 3.7 ± 0.8 memory items.

EEG was recorded with Nervus 3.2 (VIASYS Healthcare) with a sampling frequency of 256 Hz. 19 Ag/AgCl electrodes were attached onto the scalp with conductive electrode paste according to the standard 10/20 setup (with positions F_{P1} , F_{P2} , F_3 , F_4 , C_3 , C_4 , P_3 , P_4 , O_1 , O_2 , F_7 , F_8 , T_3 , T_4 , T_5 , T_6 , F_z , C_z , P_z). The reference electrode was placed next to the C_z electrode. Skin impedance was below 10 k Ω . An oculogram was recorded bipolarly between electrodes positioned directly lateral to and below the right eye. A two-electrode electrocardiogram was also recorded.

The raw EEG was digitally band-pass filtered (0.05 Hz–55 Hz) and notch filtered (50 Hz). Data was split into trials starting 1 s before the onset of the first stimulus and finishing 0.5 s after the offset of the last stimulus. The EEG data was visually inspected and epochs containing obvious artifacts related to head movements, epileptic and/or muscle activity were removed. Independent component analysis in EEGLAB (<http://www.sccn.ucsd.edu/eeglab/>) was used to clean the EEG data from artifacts. Independent components with ocular or heart artifacts were removed from the epochs, and the remaining components were mixed back

together again. Incorrect trials were left out of the analysis. After preprocessing, 23 subjects remained. The remaining sessions contained on average 27 ± 8 trials from each subject. From each EEG trial, the baseline (1.0 s–0.5 s before the onset of the first stimulus) and the last two delay period time segments of the trial were extracted from electrode pairs $F_3 \leftrightarrow P_3$ and $F_4 \leftrightarrow P_4$ for the DTF analysis. Since the vsWM testing task was adaptive, the extracted delay periods reflect a vsWM load at the capacity limit.

2.4. Calculation of inter-regional effective connectivity with the directed transfer function

The direction of the net effective connectivity between regions was calculated on both experimentally obtained, normalized EEG and simulated LFP data [16–18]. All data analysis was performed in Matlab® (Mathworks, Natick, USA). A multivariate autoregressive (Mvar) model was fitted to each time segment using the Matlab ARfit package [36] (<http://www.gps.caltech.edu/~tapio/arfit>). The Mvar model is defined as $\sum_{j=1}^p A_j X_{t-j} = E_t$, where X_t is the two-dimensional fronto-parietal EEG time series at time t , E_t is white noise and A_j is the two-dimensional matrix of model coefficients. The order p was decided automatically and independently for each time segment based on the Schwarz’s Bayesian Criterion ($p_{\text{EEG}} = 11.7 \pm 1.7$; $p_{\text{LFP}} = 54.6 \pm 7.0$ during cue or delay activity and 23.8 ± 5.7 during baseline). The magnitude of the residual after fitting of the Mvar model was less than 1% of that of the total signal, implying that the model fit was excellent. By a z -transformation of the model coefficients to obtain $H(z)$, the transfer function of the system:

$$H(z) = \left(\sum_j A_j e^{-2i\pi f dt} \right)^{-1},$$

the DTF at a specific frequency can be calculated with the equation $DTF_{ij}(f) = |H_{ij}|^2 / \sum_m |H_m|^2$, where f is the frequency. The difference $DTF_{ji}(f) - DTF_{ij}(f)$ is the net effective connectivity from electrode i to electrode j . EEG contents in the θ , α , β and γ frequency bands were calculated. The frequency bands were defined in relation to the individual α frequency or IAF ($8.2 \text{ Hz} \pm 0.84 \text{ Hz}$) as advocated by Klimesch [37]. Given the similar behavior of the band and lowest α band on the one hand and the two upper α bands on the other in vsWM tasks [38], the former two were pooled into a single θ band, whereas the latter two were pooled into a single α band. Thus, the resulting bands were defined as $\theta = \text{IAF} - 6$ to $\text{IAF} - 2 \text{ Hz}$, $\alpha = \text{IAF} - 2$ to $\text{IAF} + 2 \text{ Hz}$, $\beta = \text{IAF} + 2$ to $\text{IAF} + 22 \text{ Hz}$ and $\gamma = \text{IAF} + 22$ to $\text{IAF} + 47 \text{ Hz}$. For the statistical analysis of DTF calculations on EEG, a random effects general linear model was used to analyze the data [39]. A statistical threshold of 0.05 was used in all analyses, Bonferroni corrected for multiple comparisons due to four frequency bands and two electrode pairs ($F_3 \leftrightarrow P_3$ and $F_4 \leftrightarrow P_4$).

3. Results

The structure of the vsWM model is shown in Figs. 2(a) and 2(b). Simulations of the “symmetric hierarchic” vsWM network are shown in Figs. 2(c) and 2(d). The network starts in a resting state (we will henceforth refer to this state as “baseline”). A visual stimulus (a 0.5 s long, $1 \mu\text{A}/\text{cm}^2$ current into pyramidal cells coding for the stimulus) presented to the IPS causes the network to display persistent activity coding for the memory of the location of the cue. Due to the inter-regional connections, activity soon spreads to the SFS. During the 12 s delay period, memory is encoded by the spatially localized, persistent activity. The maximal mnemonic firing rate is low, about 25 Hz, similar to experiments. At selection, a current causes the network to return to the spontaneous state. In some trials, distracters entered the network. They were modeled as visual cues arriving during the delay period at a different angle than the cue. The simulations showed that the model accounts for several characteristics of the delay-phase neural activity in the vsWM tasks [27, 40]. As in previous, single-region, versions of the model. Model neurons showed the experimentally observed stable baseline activity during the inter-trial interval as well as stable, spatially localized and physiologically realistic mnemonic firing rates during the delay phase. The model also reproduced the decrease in activity in cells not coding for the memory during the delay phase. The activity in the two simulated regions was very similar, which is in agreement with single-unit recordings from the frontal and parietal cortices in the macaque [27].

3.1. *Inter-regional similarity of spiking activity does not imply inter-regional connection symmetry*

Recordings from behaving monkeys have demonstrated that the spiking activity in SFS and IPS is indistinguishable, such that the firing rates of neurons are not different in the two regions, and the same cell types with the same types of firing behavior (ramping, stable, decreasing, etc.) are present in the two regions [27, 41]. Does this mean that the connectivity of the two regions is also symmetric? To test this, we started out with a “symmetric” network where activity in both regions was the same. To create comparable but asymmetric networks, we then increased or decreased the local connection strength in one region while we decreased or increased the strength of the connection from the other region into this region so as to keep the total connection strength in the network constant. These changes in the effective connectivity did not affect the network firing rates (Fig. 3(a)). This means that even though the activity observed in two regions is similar, the architecture of the two regions need not be symmetric. Instead, it is the total strength of incoming local and inter-regional connections that determines the firing rate within an area.

Likewise, when the firing rate in two unconnected regions is not the same, adding an inter-regional connection can still lead to similar spiking activity in the two regions (Figs. 3(b)–3(d)). Interestingly, this indicates that one effect of

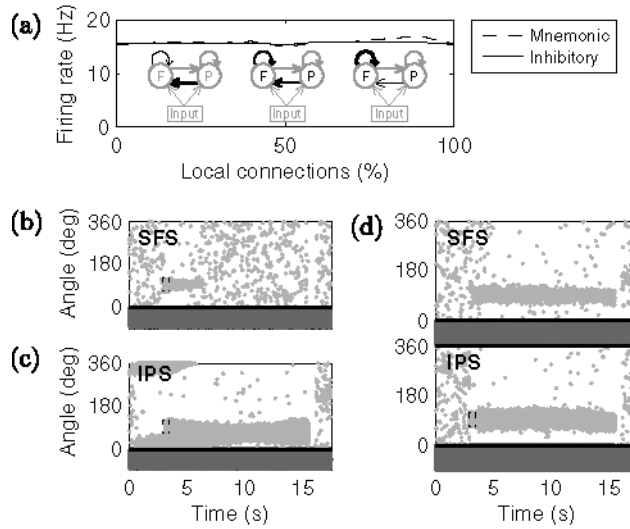


Fig. 3. Similar spiking activity in the two networks does not imply that the network is symmetric. (a) Mean firing rate in the pyramidal cells coding for the stimulus (“Mnemonic”) and in the inhibitory cells (“Inhibitory”) in the vsWM network during maintenance changes only slightly when the local connections in one area are exchanged for inter-regional connections. The cartoon networks highlight the cases corresponding to the different rows in Fig. 1. P represents the parietal region and F the frontal. The black arrows in the cartoon networks indicate the connection whose strengths were varied. Connections entering the IPS were unchanged. (b–d) Two dysfunctional networks can stabilize each other. (b) The SFS region has pyramidal-to-pyramidal connections with mean connection strength 1.2 mS/cm^2 , which is too low to sustain stable persistent activity. (c) The IPS region has pyramidal-to-pyramidal connections with mean connection strength 1.5 mS/cm^2 , which is too high to sustain stable spontaneous activity. (d) When the two networks were interconnected, they started to function, and activity was similar in the two regions.

inter-regional connections might be to stabilize activity patterns in the vsWM network. Figures 3(b) and 3(c) shows two networks that are dysfunctional, one with too strong recurrent connections for stable spontaneous activity and one with too weak recurrent connections for stable memory activity. When the networks were interconnected, both spontaneous activity and memory activity in these lopsided networks were now stable, and activity in the two regions was very similar (Fig. 3(d)). In conclusion, a simple comparison of population activity from electrophysiological recordings in two areas is not sufficient to distinguish between networks with different effective connectivity between the IPS and SFS.

3.2. The vsWM network has a “fronto-parietal” effective connectivity

3.2.1. DTF analysis of vsWM-related EEG activity

To investigate a possible fronto-parietal connection asymmetry, we measured EEG from children performing a vsWM task (Fig. 4). Figure 5 shows the power spectra of EEG activity during a baseline period and during full memory load from the

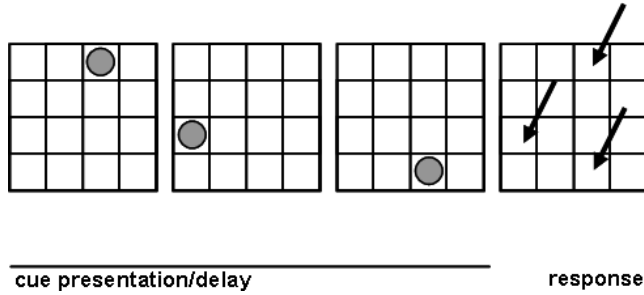


Fig. 4. vsWM test. *Cue presentation/delay*: Gray circles were presented sequentially for 1 s with 0.5 s delay periods between presentations. *Response*: After all cues had been presented, the subjects had to respond by clicking in the right order in the squares where the circle had appeared in the same order.

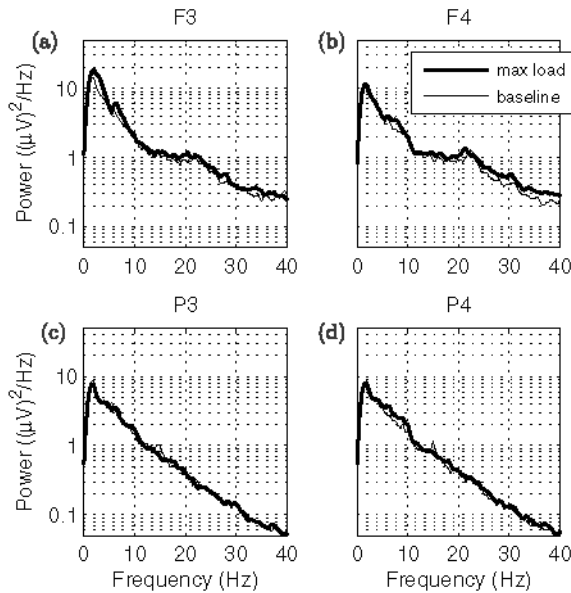


Fig. 5. Power spectra during baseline (1.0 s to 0.5 s before the first stimulus) and maximal vsWM load (the last two delay periods). (a) Electrode F₃. (b) Electrode F₄. (c) Electrode P₃. (d) Electrode P₄.

electrodes (P₃, P₄ and F₃, F₄) monitoring IPS and SFS activity. Consistent with earlier studies [41–45], we observed that the spectral power during full vsWM load was larger than or equal to the power during the baseline condition. DTFs in the P → F direction, the F → P direction as well as the net fronto-parietal DTF, (DTF_{P→F} – DTF_{F→P}), were calculated for electrode pairs F₃ ↔ P₃ and F₄ ↔ P₄ in the θ , α , β and γ frequency bands (defined in the *Methods* section) during both full vsWM load and baseline. To isolate vsWM-related DTF, our results were analyzed statistically using a random effects ANOVA model implemented in a general linear model which included the baseline and vsWM conditions. DTF was significantly

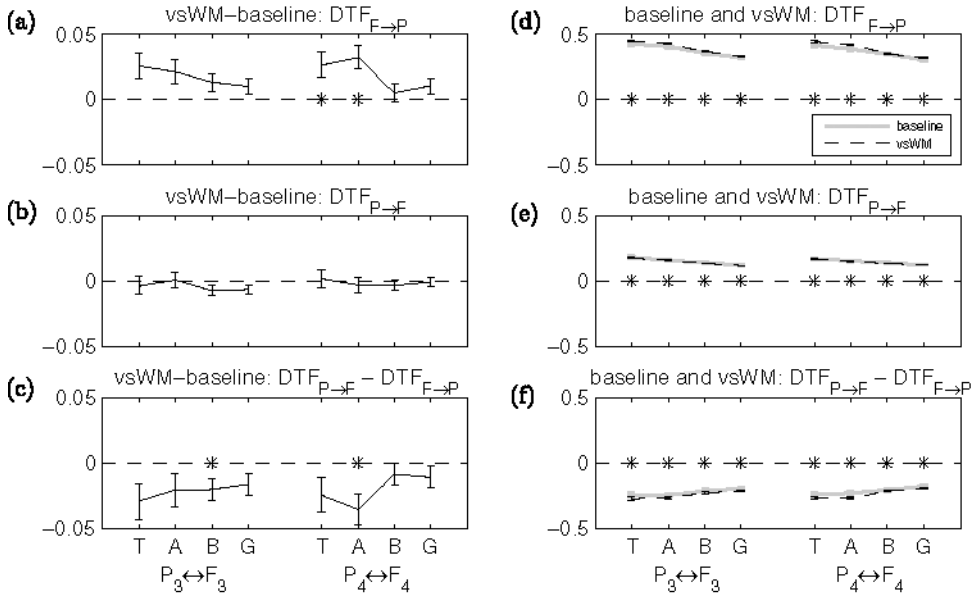


Fig. 6. DTF in different frequency bands for electrode pairs $F_3 \leftrightarrow P_3$ and $F_4 \leftrightarrow P_4$ during baseline (1.0s to 0.5s before the first stimulus) and maximal vsWM load (the last two delay periods). (a) vsWM - baseline $DTF_{F \rightarrow P}$. (b) vsWM - baseline $DTF_{P \rightarrow F}$. (c) vsWM-related $DTF_{P \rightarrow F} - DTF_{F \rightarrow P}$. (d) $DTF_{F \rightarrow P}$ for vsWM and baseline. (e) $DTF_{P \rightarrow F}$ for vsWM and baseline. (f) $DTF_{P \rightarrow F} - DTF_{F \rightarrow P}$ for vsWM and baseline. (c-e) Black: vsWM. Gray: baseline.

stronger during vsWM than baseline from $F_4 \rightarrow P_4$ in the θ and α frequency bands ($P < 0.05$) (Fig. 6(a)), whereas no significant effect was found in the connection from $P_4 \rightarrow F_4$ (Fig. 6(b)). A significant increase in fronto-parietal net DTF during vsWM ($DTF_{P \rightarrow F} - DTF_{F \rightarrow P} < 0$) was found in the $F_3 \leftrightarrow P_3$ pair in the β band and in the $F_4 \leftrightarrow P_4$ pair in the α band ($P < 0.05$) (Fig. 6(c)). Note that the DTF results were similar across all electrodes and frequency bands although statistical significance was only observed in some cases (Figs. 6(a)–6(c)). DTFs were also calculated during conditions baseline and vsWM only without comparison (Figs. 6(d)–6(f)). In all frequency bands, $DTF_{F_3 \rightarrow P_3}$, $DTF_{F_4 \rightarrow P_4}$, $DTF_{P_3 \rightarrow F_3}$, $DTF_{P_4 \rightarrow F_4}$ were significantly larger than zero in both conditions, and the differences $DTF_{F_3 \rightarrow P_3} - DTF_{P_3 \rightarrow F_3}$ and $DTF_{P_4 \rightarrow F_4} - DTF_{F_4 \rightarrow P_4}$ were significantly smaller than zero for both conditions.

3.2.2. Computational analysis of relation between connectivity and DTF

To study the relationship between effective connectivity and DTF as well as how the DTF is affected by biophysical factors, we calculated the DTF from model simulations. Simulated LFP power, coherence spectra and firing rates from the two regions during baseline, cue presentation and WM delay are shown in Figs. 7(a)–(d). Generally, the firing rate was higher during the vsWM delay condition than during baseline, and higher still during cue presentation (Fig. 7(a)). This was also true of LFP power (Fig. 7(b)) and inter-regional coherence (Fig. 7(c)), and neither the

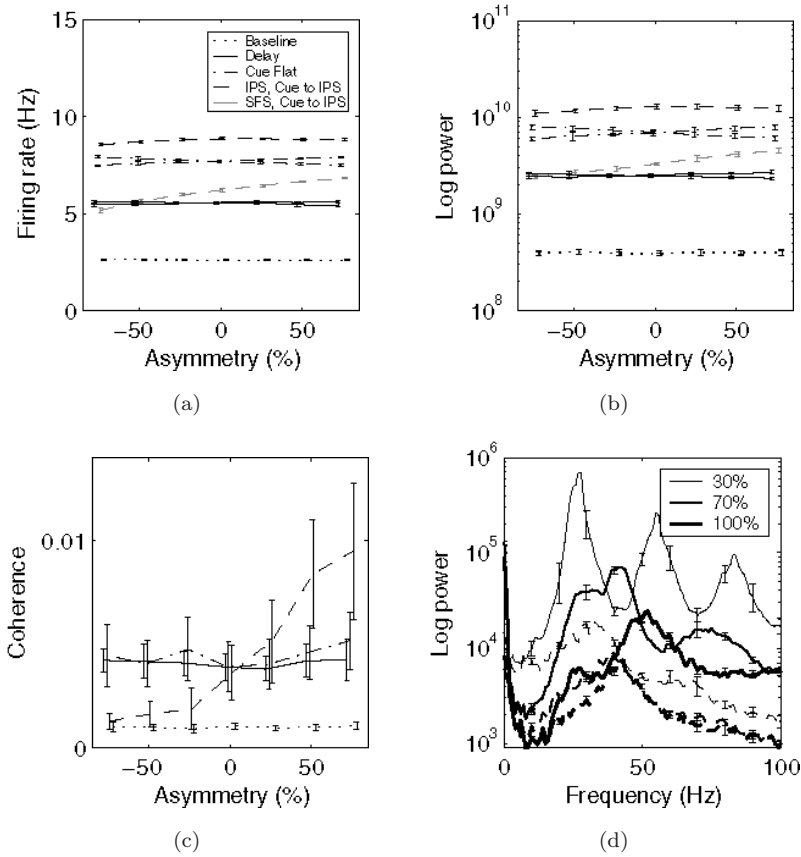


Fig. 7. Simulation of vsWM-related EEG signals. (a) Average firing rates across all cells for networks with 70% NMDA and with different degrees of asymmetry during rest, WM delay and cue presentation in the two regions. Inter-regional connection asymmetry was varied from -100% to $+100\%$, where $\pm 100\%$ means that all inter-regional connections go in one direction, and 0% means that connections are equally strong in both directions. Rates are independent of the degree of inter-regional asymmetry, except that frontal firing rates during cue presentation to the IPS increase with the degree of inter-regional asymmetry. (b) Summed spectral power for the same networks as in (a) was higher during delay than rest and higher still during cue presentation. During cue presentation to the IPS, power in the frontal region was higher in more parieto-frontal networks. Apart from that frontal power increases with the degree of inter-regional asymmetry during cue presentation to the IPS, no dependency of the power spectra on the degree of asymmetry is seen. (c) Coherence for the networks as in (a) shows the same pattern as the power spectra, having the smallest coherence at rest and larger coherence during vsWM delay and cue presentation as well as not depending on inter-regional connection asymmetry except for during cue presentation to IPS. (d) Effect of NMDA ratio on power spectrum appearance. Delay-phase power (thick solid lines) is larger than resting-phase power (thin, dashed lines) in the γ band for all values of the NMDA ratio. Error bars indicate the sample standard deviation ($n = 12$ simulations for each data point).

firing rate, nor the LFP power or coherence, showed any dependence on inter-regional asymmetry except during cue presentation to the IPS only. During that condition, the firing rate in the IPS was increased by the incoming cue [black line in Fig. 7(a)]. The elevated activity in IPS in turn caused an increase in the firing rate in SFS, an

effect which was stronger when $\text{IPS} \rightarrow \text{SFS}$ connection strength was high. Although the shape of the spectrum is quite dependent on the NMDA (*N*-methyl-D-aspartic acid) ratio (the percentage of recurrent excitatory connections that are of the NMDA type), the γ power is relatively stronger during delay compared to baseline and during cue presentation compared to delay for all tested values of the NMDA ratio [Fig. 7(d)], as has been found in previous studies on WM [41–43]. This is also in line [46, 47] with the increased fMRI signal during WM delay in both experiments and in simulations in this model [14]. From this analysis, we therefore conclude that neither the power spectra, firing rate or the coherence can indicate the degree of IPS–SFS connection asymmetry.

In contrast to the computational model, where all activity originates from local neuronal circuits in IPS and SFS, experimental EEG measurements contain vsWM-related activity originating largely in the IPS–SFS network (found at both high and low frequencies) and activity involving other structures as well, for example the thalamus (found mostly at low frequencies). In addition, EEG measurements also include activity from surrounding brain tissue unrelated to the vsWM task. Therefore, a close comparison of the power spectrum generated from the model and the experiments is expected to reveal both similarities and dissimilarities. Indeed, the spectral power is higher during full vsWM load than baseline in both the model and experiments [cf. Figs. 5 and 7(d)]. Yet, this difference is much larger in the model, which most likely reflects the fact that the model only includes vsWM-related cells, whereas the majority of cells contributing to the experimentally recorded EEG are unrelated to any vsWM function causing a smaller effect in the EEG power spectra. The overall shape of the spectrum is also different between model and experiment. Most EEG activity in experiments is concentrated in the lower frequency bands (θ , α), whereas the activity in the model is mostly found in higher frequencies (β , γ) [cf. Fig. 5 and Fig. 7(d)]. Again, this difference between model and experiment was to be expected, because activity in higher frequency bands is thought to be generated mostly by local circuit mechanisms, whereas activity in lower frequency bands are generated both locally and globally (involving, for example, the thalamus). This means that the model cannot be expected to predict DTF in lower frequency bands, since that activity could have been caused by mechanisms not incorporated in the model in addition to those in the model. It is important to bear in mind, however, that although the model cannot predict the DTF at lower frequencies, it does not mean that the local mechanisms explored in this study do not contribute to the DTF. More research is needed before conclusions can be made regarding the mechanisms behind the DTF changes in lower frequency bands, since the mechanisms behind low frequency oscillations in the brain are far from being understood.

The lack of dependence between asymmetry and power spectra, firing rate and coherence means that they cannot be used to investigate inter-regional asymmetry. Instead, we calculated the DTF during WM delay, cue presentation and baseline in a network where the internal structure (the number of cells, types of ion

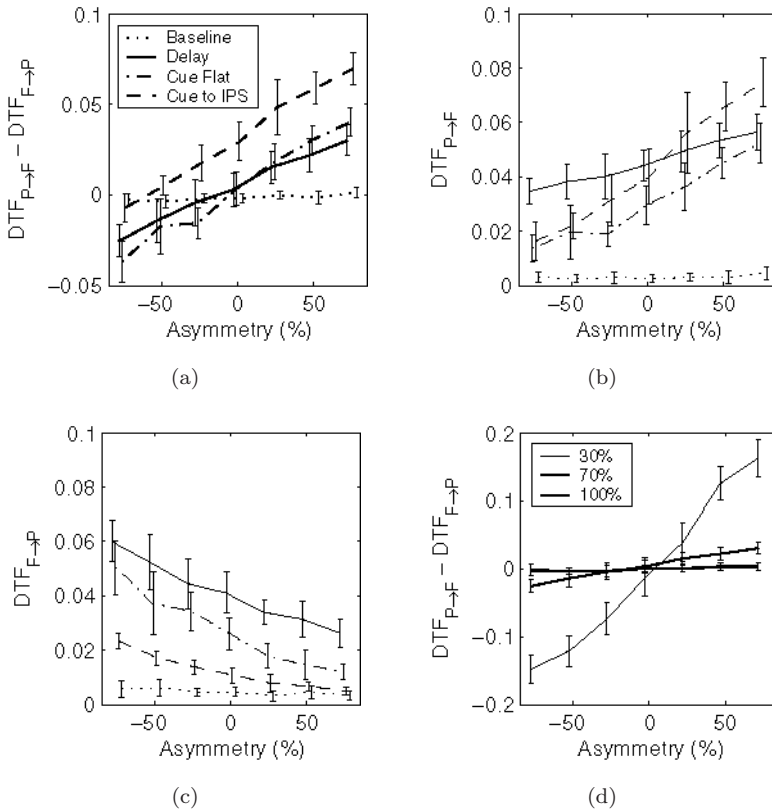


Fig. 8. Mean DTF averaged across oscillation frequencies for the networks in Fig. 5. (a) Net parietal-to-frontal flow increases with connection asymmetry for all task phases except for rest in networks with 70% NMDA. For “symmetric” networks, net flow is zero unless a cue is presented to the IPS, in which case the DTF is shifted to more positive values; (b) Parietal-to-frontal flow increases with connection asymmetry; (c) Frontal-to-parietal flow decreases with connection asymmetry. From (b) and (c) is apparent that the increased net flow during cue presentation to IPS is caused by decreased frontal-to-parietal flow rather than increased parietal-to-frontal flow. (d) As the NMDA ratio is varied from 30% to 100%, the slope of the DTF decreases. Error bars indicate the sample standard deviation ($n = 12$ simulations for each data point).

channels, NMDA ratio, etc.) of the two regions was identical [Figs. 8(a)–8(d)]. The DTF accurately described the connectivity such that “parieto-frontal” networks have more positive DTF values and “fronto-parietal” networks have more negative DTF values [Fig. 8(a)]. During WM delay, baseline and the presentation of a cue to both regions, the DTF is simply a multiple of the degree of asymmetry in the network, whereas cue presentation to the IPS results in a more parietal-to-frontal DTF. Although the magnitude of the DTF is dependent on the NMDA ratio [Fig. 8(d)], the general relationship between connectivity and DTF is not. However, as the NMDA ratio approaches 1, the DTF goes to 0, presumably because the extremely long time scale of the NMDA channels causes the network to desynchronize.

Comparing the results of the computational model to the experimental results, we see that the experimentally observed negative value of the net DTF ($\text{DTF}_{\text{P} \rightarrow \text{F}} - \text{DTF}_{\text{F} \rightarrow \text{P}} < 0$) was found in the “fronto-parietal” network only (first row in Fig. 1). Note however, that not even the DTF of the “fronto-parietal” network behaves exactly like the experimentally observed DTF: the experimental $\text{DTF}_{\text{P} \rightarrow \text{F}}$ is not different from zero, whereas $\text{DTF}_{\text{P} \rightarrow \text{F}}$ during vsWM is always larger than during baseline in the model. This difference is most likely due to the very low activity in the model pyramidal cells during baseline. In theory, fronto-parietal asymmetry should be measurable and similar regardless of activity level (compare, for instance, the delay and flat cue conditions in the model (Figs. 7 and 8)), but with the pyramidal cells silent during baseline, the two regions are effectively isolated from each other. However, this is a limitation of the model and baseline activity in vsWM-related cells is higher in experiments [40]. So if we believe that DTF calculated from vsWM network activity during baseline and vsWM should give the same results in experiments, why then do we perform a comparison to baseline? This is because the experimentally measured activity contains both activity in the vsWM network and activity in other adjacent local circuits. During vsWM delay, the activity in the vsWM network is higher and thus represents a larger proportion of total network activity. Therefore, a comparison to baseline activity makes sense in the experiments although it does not make sense in the model. Finally, note that the comparison to baseline in the experimental case only informs us that the vsWM network has a more “fronto-parietal” net DTF than the surrounding brain networks active during baseline but is inconclusive about the network structure. By only considering the experimental DTF during baseline [Fig. 6(d)–6(f)], we observe that the baseline network has a “fronto-parietal” net DTF, suggesting that the isolated vsWM net DTF is also “fronto-parietal”.

For the simple case when the two regions are identical, the DTF is related to connection strength in a simple fashion. However, it is not clear how to interpret DTF data when the two regions are asymmetrical. There are at least two differences between SFS and IPS suggested by the preceding analysis of the simulated and experimental data that could affect the relationship between effective connectivity and DTF, namely the NMDA ratio in inter-regional connections and γ -band power. An inspection of experimental power spectra indicates that parietal power was about 2.5 times lower than frontal power in the range from 30 Hz to 55 Hz ($\gamma_{\text{P}}/\gamma_{\text{F}} = 0.38$), something that could have been caused by SFS–IPS differences in the intra-regional NMDA ratio, since more AMPA (α -amino-3-hydroxy-5-methyl-4-isoxazolepropionic acid) leads to stronger high-frequency fluctuations (although there are several ways in which γ band activity can be changed). To test the effect of lower parietal synchronization, we started with a “reference” network with an NMDA ratio of 70% and lowered parietal γ power by increasing the intra-regional NMDA ratio of the IPS to 85%. Figures 9(a)–9(d) shows power spectra and DTF of the resulting network (“intra”) and the reference network. In comparison with

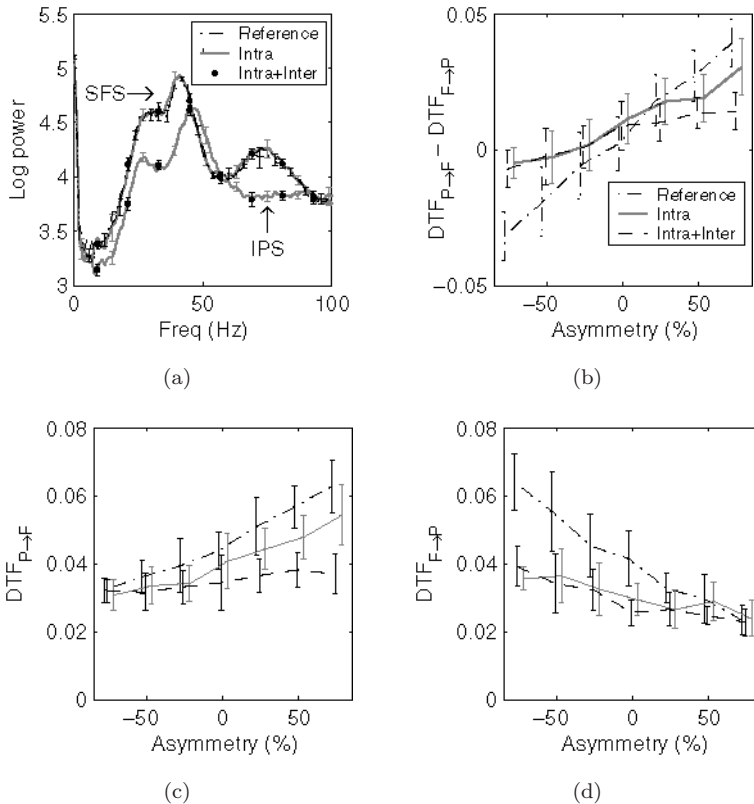


Fig. 9. The effect of a SFS-IPS difference in NMDA ratio on DTF. DTFs were calculated from a symmetrical reference network with NMDA ratio 70% (“Reference”, cf Fig. 6), a network with 85% NMDA in IPS intra-regional connections (“Intra”) and a network with 85% NMDA also in the connection from IPS to SFS (“Intra + Inter”). (a) Frontal and parietal power spectra. The frontal power spectra of the three networks are almost identical, whereas the parietal power spectra are lower for the “Intra” and “Intra + Inter” networks. (b) DTF as a function of asymmetry. (c) Frontal to parietal flow of information (d) Parietal to frontal flow. Error bars indicate sample standard deviation ($n = 12$ simulations for each data point).

the reference network, the “intra” network has a flatter DTF curve that crosses the zero line at -25% or -50% asymmetry (“fronto-parietal” networks). The discrepancy between the DTF and the connection strength in the network seems to be caused primarily by a lower DTF from SFS to IPS, although the DTF for the connection from IPS to SFS also decreased [Figs. 9(c)–9(d)]. We next tested whether an increased inter-regional NMDA ratio (“Intra + Inter”) would affect DTF measurements. We therefore increased the NMDA ratio in the SFS \rightarrow IPS connection to 85%. This caused the DTF curve to flatten out further, but the position where the DTF was zero remained at -25% or -50% . The main effect of the two fronto-parietal asymmetries on the DTF curve was therefore that they cause moderately “fronto-parietal” networks to produce DTFs of zero. This shows that the interpretation of the DTF without taking biophysical factors into account can lead one

to reach erroneous conclusions regarding network effective connectivity. Comparing simulated and experimental DTF, it is clear that only “fronto-parietal” networks had DTFs commensurate with the experimentally measured DTF. We therefore conclude that the working memory network is “fronto-parietal”.

3.3. The vsWM network has a “hierarchical” structure

Even though the analysis thus far suggests a “fronto-parietal” organization between IPS and SFS, we cannot yet determine how visual stimuli (including distracters) enter the vsWM maintenance network, i.e. if the network is hierarchic or flat (Fig. 1). For this purpose, we studied the distractibility of the “symmetric” model network as a function of the inter-regional effective connection strength (Fig. 10). Distracters were modeled as cue stimuli entering the network during the delay period at a different angle than the original stimulus. Total connection strength was fixed, and hence, so was the spiking activity in the network (cf. Fig. 3). According to Sakai *et al.* [15], inter-regional correlations of neural activity as measured with fMRI (a sign of inter-regional connection strength in this model [14]) are correlated with improved resistance against distraction, even when total neural activity is constant. This is indeed the case when stimuli enter the IPS only. However, when stimuli enter both regions with equal intensity, stronger inter-regional connections do not offer protection against distraction (Fig. 10). The fMRI data from Sakai *et al.* [15] therefore support the dorsal stream hypothesis. We can conclude that the comparison between experiment and simulation regarding distracter processing supports the “hierarchic symmetric” network in Fig. 1.

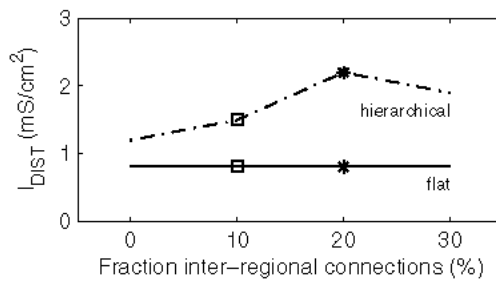


Fig. 10. Distractibility as a function of effective connection distribution. The fraction of inter-regional to total pyramidal-to-pyramidal effective connection strength was varied in the model while total effective connection strength was kept constant. Distractibility was measured as the minimal stimulus amplitude (mS/cm²) needed to cause the network to lose memory of the position of the stimulus in at least one region. When distracters entering both regions were equally strong, distractibility was not dependent on the connection distribution (solid line). When distracters only entered the IPS, then more effective inter-regional connections offered a stronger protection to distracting stimuli (dash-dotted line). Note that when distracters entered the IPS only, the average intensity required to distract memory activity was approximately doubled, since only one distracter was presented.

3.4. “Fronto-parietal” networks protects against visual distraction

The importance of the SFS–IPS connection for distractibility indicates that asymmetry in this connection could also affect network distractibility. Although we have just concluded that the vsWM maintenance network of healthy adults is “fronto-parietal”, it is possible that the vsWM network of people with good and poor vsWM could have a different effective connectivity. We therefore varied the degree of asymmetry of the effective inter-regional connection strength in the model and measured distractibility. Figure 11 shows, that for the hierarchic networks, the “fronto-parietal” network is more resistant against distraction than the “symmetric” or “parieto-frontal” networks. If the IPS were to be distracted, a low IPS \rightarrow SFS connection strength protects against the distraction of the SFS. Further, a strong SFS \rightarrow IPS connection protects the IPS from being distracted in the first place. Conversely, if the IPS \rightarrow SFS connections are the strongest, then the network is even less resistant to distraction than the “symmetric” network. Therefore, this shows that SFS–IPS asymmetry affects working memory performance and indicates a way to redistribute inter-regional connections in order to increase the resistance against distraction.

3.5. Conclusion

In conclusion, we found one configuration of the network that could explain not only the experimentally obtained value of the directed transfer function of EEG activity during the delay period, but also the experimentally observed protection against distracters offered by effectively stronger inter-regional connections. This was the “hierarchic fronto-parietal” network in Fig. 1, into which cue and distracter stimuli enter only through the IPS, and in which the SFS \rightarrow IPS connection was stronger than the IPS \rightarrow SFS connection. The protection against distraction offered by stronger SFS–IPS connections was due to SFS activity stabilizing activity in IPS challenged by distracters. Hence, it was primarily stronger SFS \rightarrow IPS connections

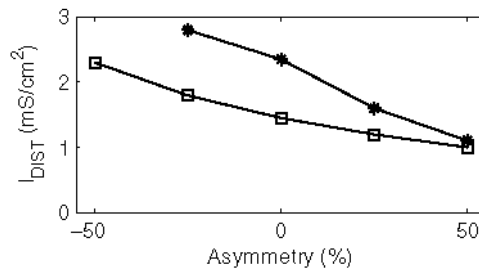


Fig. 11. Distractibility in the hierarchic network as a function of asymmetry in the SFS–IPS connection. Distractibility was measured as in Fig. 8. Strong SFS \rightarrow IPS connections and weak IPS \rightarrow SFS connections endow the network with higher resistance to distracters, whereas if connection strengths are reversed, then the network becomes more distractible. Squares indicate 10% inter-regional connection strength of total strength, stars 20%.

that protected against distraction, whereas stronger $\text{IPS} \rightarrow \text{SFS}$ led to poorer distracter resistance. The model therefore predicts that a difference in the asymmetry of the vsWM network could be found in people with different vsWM performance.

4. Discussion

In this study, we determined the effective connectivity of the fronto-parietal vsWM network, and whether differences in effective connectivity have functional consequences for vsWM mnemonic stability. To study this problem, we employed a new approach, where we used a biophysically-based computational model to analyze EEG data collected during the performance of a vsWM task. Recently, we used the same method successfully to causally relate developmental changes in the structure of the fronto-parietal vsWM network during childhood to changes in brain activity and vsWM capacity [10]. Although others have also used biophysically based models for the analysis of large-scale brain activity measured with fMRI, positron emission tomography or EEG [48,49], these studies have not specifically investigated the role of biophysical factors on calculations of effective connectivity. Using our integrated approach, we determined that the vsWM network is asymmetric with stronger $\text{SFS} \rightarrow \text{IPS}$ connections than $\text{IPS} \rightarrow \text{SFS}$ connections. Next, we performed model simulations to show that visual stimuli enter the vsWM network via the IPS only. Having thus found that a “hierarchical fronto-parietal” network best fits experimental data, we performed additional model simulations to understand the mechanism whereby the SFS – IPS connection protects against distraction. We demonstrate that this effect is mostly caused by strong $\text{SFS} \rightarrow \text{IPS}$ connections, whereas $\text{IPS} \rightarrow \text{SFS}$ connections have the opposite effect on resistance against distracters.

By using the biophysically-based model to test the effect of biophysical factors on the DTF, we showed that the interpretation of the DTF is not trivial when the structure of the underlying network is not well specified. It is well known that correlations between activity in different brain regions can be driven by an external brain region, and in case the external region is not included in the model, spurious connections between the two brain regions can arise (see e.g. [18]). Here, we show that even in the simple case of a two-region network, it is not straightforward to draw conclusions about the effective connectivity if the biophysical characteristics of the model are not well specified. By taking into account the effect of inter-regional differences in γ band activity and possible differences in the NMDA ratio of inter-regional connections on the magnitude of the DTF, we reached the unintuitive conclusion that a symmetric DTF between the SFS and IPS can be caused by an asymmetric “fronto-parietal” network. Our approach is extendable in the sense that if additional differences in biophysical properties between the SFS and IPS are identified, they can easily be incorporated and analyzed according to the scheme outlined in the present study.

To the best of our knowledge, the effective connectivity of the vsWM network has only previously been studied by Babiloni *et al.* [16]. They found no difference

between SFS \rightarrow IPS and IPS \rightarrow SFS DTF during the delay period, as opposed to the fronto-parietal network found in our task. There could be several reasons for this discrepancy. First, there is a difference in tasks between the different studies, mainly in difficulty level, where Babiloni only used a WM load of one item, which only poses minimal demands on WM. Future studies on the effect of load on directionality could therefore be of interest. Second, the conclusions from Babiloni *et al.* [16] could be modified by the computational analysis performed in the present study. Given that the frontal/parietal γ power ratio is about the same in their study as in ours, our computational analysis indicates that a “fronto-parietal” network produces the symmetric DTF found in their study, in which case the two studies arrive at the same conclusion. This further underlines the utility of a combined computational and experimental approach when studying the relationship between network structure and function.

Sakai *et al.* [15] demonstrated that inter-regional correlations were important for the ability to resist distraction. Here, we show two ways by which strong connections can stabilize vsWM. For “hierarchical” networks, which we concluded represent actual vsWM network connectivity better than “flat” networks, stronger inter-regional connections protect against distraction (Fig. 10). This turned out to be because the SFS \rightarrow IPS connection helps stabilize mnemonical activity in the IPS (Fig. 11). On the other hand, the IPS \rightarrow SFS connection seemed to destabilize memory activity by allowing distracters to reach the SFS. In addition to the importance of effective connectivity for distracter resistance, we also found that two networks which on their own could not maintain stable spontaneous or mnemonic activity could do so when they were interconnected (Fig. 3). There are two implications from this. First, if one of the regions is afflicted with disease or injury, then memory activity in that region may be stabilized by the activity in the other region, which would not have been possible had the network contained only one region. Second, and possibly more importantly, it limits the understanding we can hope to get from studying just one part of a network at each time, as is done in most neurophysiological experiments.

The results in Figs. 10 and 11 could also be obtained by adjusting the height of the connection curve J^+ of the IPS \rightarrow SFS and SFS \rightarrow IPS connections (data not shown). This is an example where a change in effective connectivity (a functional measure) is achieved without a change in total connection strength (a structural measure), and is in line with the conclusions from our previous study [14], where the increased connection strength between *active* cells in the network, regardless of whether it was caused by a change in total connection strength or J^+ , led to higher inter-regional correlations and mean network spiking activity and thereby increased ability to resist distraction.

With regard to the conclusion that the vsWM is hierarchical, it should be noted that the time it takes for IPS to activate SFS in the model, hundreds of milliseconds [Fig. 2(d)], may appear somewhat long. In single cell recordings, Chafee and Goldman-Rakic [27] observed a non-significant trend that cells in area 8a are

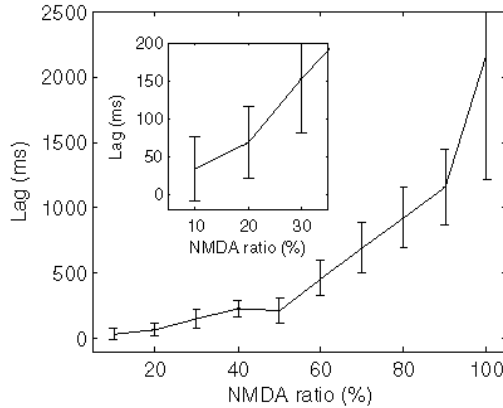


Fig. 12. Time lag of activation of the SFS is a function of the NMDA ratio of the excitatory connections. The higher the AMPA ratio, the shorter is the lag in activation of the SFS. Ten simulations were done with the “symmetric hierarchical” network for each NMDA ratio. A sigmoid function was fitted to the population activity of each region. The region was considered to be activated at the time when the fitted sigmoid function had reached 80% of its maximal value. Error bars indicate sample standard deviations.

activated a mere 11 ms after cells in area 7ip, whereas Halgren *et al.* [50] did not observe any difference at all in an EEG study in humans. Even when decreasing the NMDA ratio to shorten this time, one cannot obtain such short activation times (Fig. 12). This indicates that the SFS is not activated by the IPS only but that the two regions are simultaneously activated by other visually responsive neural populations. However, even if there exists a weak connection from lower visual areas to the SFS, our results regarding the relation between fronto-parietal connection strength and distractibility (Figs. 10 and 11) unambiguously show that the major flow of information into the SFS goes via the IPS.

Addressing the biological plausibility of the computational model, we have assumed that the dominant interaction between the two regions is mediated by their pyramidal cells. This assumption is most likely an oversimplification since excitatory cells could make long-range connections to inhibitory cells. However, since the net effect of SFS–IPS connections is primarily excitatory [41], the relationship between distractibility, connectivity and the DTF is most likely not different from what we found in our analysis, unless there is a large difference between the IPS \rightarrow SFS and SFS \rightarrow IPS connections in the proportion of long-range synapses onto inhibitory interneurons. There is ample biological evidence justifying our assumption that the vsWM maintenance network to a first approximation consists of the IPS and the SFS.

A further assumption in this study is that the vsWM maintenance network consists of only the IPS and the SFS [9, 27, 51, 52]. Based on this, the DTF connectivity analysis was performed on the electrode pairs $F_3 \leftrightarrow P_3$ and $F_4 \leftrightarrow P_4$. However, it is well known that several regions of the brain are active during the vsWM delay period, and they could affect our results by acting as hidden nodes

leading to spurious connections in the experimental analysis. Most importantly, we cannot exclude subcortical structures such as the mediodorsal nucleus of the thalamus as constituting a major pathway of crosstalk between the IPS and SFS. Such subcortical structures are especially likely to affect the results of the DTF in the lower part of the frequency spectrum. Other methods are needed to probe the effective connectivity to subcortical structures.

In this study, we have proposed one mechanism based on fronto-parietal connection asymmetry, whereby the stability of vsWM activity can be improved, and have compared simulation results to experimental data. Naturally, this mechanism is only one of several mechanisms which work to improve vsWM stability. In a previous study, we have shown that increases in total connection strength leading to increased firing rate also stabilizes vsWM activity [14]. In that article, an increase in the SFS–IPS connection strength was identified as the mechanism leading to improved working memory during childhood, but other mechanisms, such as a change in the frontal network input-output curve [53] or cellular bistability [54], making the memory state a stronger attractor, would also lead to improved vsWM (without necessarily increasing neuronal firing rates). In a companion study of the same data set, we investigated the effect of distraction on brain activity in children and adults [55]. That study found that distracters cause activation in occipital areas and IPS in both children and adults, but that distracter-related activity in the SFS was found only in children. The consistent activation of IPS in both groups supports the hierarchical network configuration found in this study. The present study also indicates that the decreased distractibility in adults in that study could be partially caused by a shift towards a more “fronto-parietal” type of effective network connectivity. However, since there was a simultaneous increase in total connection strength [14], the effects of a redistribution of connections without increased total connection strength cannot be determined from that data. Interestingly, in both the study by Olesen *et al.* [55] and Sakai *et al.* [15], higher distracter resistance was associated with higher activity in the dorsolateral prefrontal cortex. It seems that the dorsolateral prefrontal cortex dynamically modulates inter-regional connection strength. It will be of great interest to understand the mechanisms whereby the dorsolateral prefrontal cortex exerts its influence on the SFS–IPS connection.

One could conjure up many possible differences between the internal structure of the SFS and IPS by changing the internal connectivity and biophysical properties within the two brain regions. The conclusion drawn in this paper that the vsWM network is “fronto-parietal” could therefore be modified by future knowledge regarding the biophysical characteristics of IPS and SFS. Our computational modeling analysis has exposed the complexity of the problem of making inferences regarding cortical connectivity from indirect measures of brain activity such as EEG and fMRI, and this in itself is a step forward from drawing conclusions directly from the DTF (or other analysis methods). We have identified two factors which affect the relationship between the effective connectivity and the DTF, namely the

internal oscillatory behavior of the studied brain regions and the NMDA ratio of the connections between them. Experiments should be conducted to identify the NMDA ratio and the contributions of the relevant neural populations to the EEG oscillations. To truly solve the connectivity puzzle, however, a more principled and comprehensive approach should be employed where one tries to combine as much information as possible about the factors that affect network activity. This would involve collecting the most informative data types and evaluating that data with analysis methods taking the complexity of the data into account. For example, intracranial spiking and LFP recordings from several cortical and subcortical locations could be combined with a computational model incorporating up-to-date knowledge about the relationship between spiking and LFP activity based on the biophysical characteristics of each region. Based on the mechanistic model, a suitable non-linear statistical model could then be designed to evaluate hypotheses. With this approach, model predictions could also be validated by perturbation analyses, such as cooling [41], pharmacological blocking or electrical stimulation. In the long run, such a comprehensive approach could end up being the fastest and cheapest way to solve the complex problem explored in this study.

The following predictions concerning the relationship between effective connectivity and distractibility could be tested experimentally under different conditions: (i) stronger inter-regional effective connectivity (in particular SFS \rightarrow IPS connections) should cause higher resistance against distraction; (ii) stronger maintenance-related activity in the IPS should also cause higher distracter resistance, since stimuli enter primarily along the dorsal stream; (iii) distracter resistance should be correlated to the product of SFS activity and SFS \rightarrow IPS connection strength, since the influence of SFS activity on IPS activity during distraction is related both to its magnitude (the more supporting activity, the better) and to the SFS \rightarrow IPS connection strength (the stronger the connection, the larger the influence of SFS activity in the IPS).

Appendix. Supplemental Methods

A.1. Neurons

The pyramidal cell model was taken from Tegnér *et al.* [32]. It is of the Hodgkin-Huxley type and is biologically realistic insofar as it reproduces neuronal input-output curves and the shape of axonal and dendritic spikes measured in cortical slice experiments [56, 57]. The shape of the input-output curve is perhaps the most important factor for determining the stability of low mnemonic activity in the network [53], the other one being the slow dynamics of the NMDA channel [58]. The robustness of the model was assessed in Edin *et al.* [14], where synaptic locations were changed, dendrites were removed, and all but the Na⁺- and K⁺-ion channels were removed without affecting the results of that study. The inhibitory interneuron model, originally developed in [59], was exactly as in Tegnér *et al.* [32].

A.2. Synapses

Pyramidal cell synapses were of the NMDA and AMPA type, interneuronal synapses were of the GABA_A type, and background activity from the rest of the brain entered through AMPA synapses. The synapses were as in Tegnér *et al.* [32], except for the following differences. All differential equations describing the synaptic conductances were of first order to speed up computations [60]. This formulation is slightly different from that in Tegnér *et al.* [32], but the post-synaptic currents of the synapses were fitted to those in Tegnér *et al.* [32]. For the NMDA channel, such a fit can only be optimal for one frequency, chosen to be 30 Hz, but the error across frequencies is small.

For recurrent synapses (between cells in the network), the fraction of open channels s_{ij}^n and the resulting synaptic current I_{ij}^n flowing from cell j to cell i through synapse type $n = \{\text{GABA}_A, \text{AMPA}, \text{NMDA}\}$ were governed by the equations:

$$\frac{ds_{ij}^n}{dt} = \begin{cases} \alpha_n(1 - s_{ij}^n) - s_{ij}^n/\tau_n, & t_{AP} \leq t \leq t_{AP} + c_n^{\text{dur}} \\ -s_{ij}^n/\tau_n, & \text{otherwise} \end{cases}$$

$$I_{ij}^n = g_{ij}s_{ij}^n(V_i - E_n).$$

Here, $c_n^{\text{dur}} = 0.4, 2.0$ ms, $\alpha_n = 12.0, 0.3$ ms⁻¹ and $\tau_n = 10, 2, 100$ ms, respectively, and t_{AP} is the time of arrival of a spike. τ_n is the decay time constant of synapse type n . α_n and c_n^{dur} were chosen to achieve an optimal fit to the synapses in Tegnér *et al.* [32]. They are closely related to the channel opening rate and duration of transmitter in the synaptic cleft, respectively, but values might deviate slightly from values in the literature due to the reduction of the differential equations to first order. The connection strength from cell j to i , g_{ij} , is described in the *Network architecture* subsection below.

Recurrent excitatory synapses were a mix of NMDA and AMPA synapses. Connection strengths were tuned to obtain an NMDA ratio of 85% (85% of the total recurrent excitatory current in the network during memory maintenance was through NMDA channels) unless stated otherwise. We define the NMDA ratio x as the time average during vsWM maintenance of the NMDA current to total recurrent excitatory current, or equivalently, the ratio of charges, r_C . The experimental value of r_C was calculated from data from Watt *et al.* [61], as follows. For both channels, we assume a double exponential model for the synaptic current, $I_{\text{SYN}} = \exp\{-t/\tau_{\text{RISE}}\} - \exp\{-t/\tau_{\text{DECAY}}\}$. For the AMPA channel, $\tau_{\text{DECAY}} = 3.1$ ms and the 20–80% rise time = 0.8 ms, experimentally. To achieve this rise time, we set $\tau_{\text{RISE}} = 1.4$ ms. Experimental values for the NMDA channel were $\tau_{\text{DECAY}} = 150$ ms and the I_{NMDA} peaked after 15 ms. To achieve this peak time, we set $\tau_{\text{RISE}} = 4$ ms. With these values, the ratio of peak currents $r_I = I_{\text{NMDA}}/I_{\text{AMPA}} = 3.09$, and the ratio of total EPSC charge $r_C = C_{\text{NMDA}}/C_{\text{AMPA}} = 86.13$, giving a conversion factor $k = 27.8$ from r_I to r_C . In [61], the ratio of peak currents $r_I = I_{\text{NMDA}}/I_{\text{AMPA}} = 0.23$, so the NMDA ratio, i.e. the charge ratio, $r_C = kr_I = C_{\text{NMDA}}/C_{\text{AMPA}} = 6.4$, or $C_{\text{NMDA}}/(C_{\text{AMPA}} + C_{\text{NMDA}}) = 86\%$.

A.3. Network architecture

The vsWM model was composed of a frontal and a parietal region, each consisting of 128 pyramidal cells and 32 inhibitory interneurons. Each pyramidal cell encodes an angle θ in the visual field. The connection strength of pyramidal cell j onto pyramidal cell i in populations x and y (either frontal or parietal pyramidal cells) and coding for stimuli at angles θ_i and θ_j was $g_{ij} = g(\theta_j - \theta_i) = G_{xy}W(\theta_j - \theta_i)$, where $W(z) = J^+ + (J^+ - J^-) \exp\{-z^2/2\sigma^2\}$. G_{xy} is the mean connection strength from region y to x . By $g(z)$, we denote the connection curve (Fig. 2(b)). $W(x)$ describes the shape of the connection curve. The total area under $W(x)$ is kept constant by adjusting J^- to accommodate for changes in the peak J^+ and standard deviation σ of the connection curve. This means that we can increase J^+ and decrease σ in simulations without changing the total connection strength between cell populations x and y . All other connections in the network followed a flat distribution (x and y not both pyramidal cell populations). In all simulation experiments, the network regions were connected only through their pyramidal-to-pyramidal cell connections. Intra-regional connections were instantaneous while there was a delay in the inter-regional connection of 8 ms, based on measured SFS–IPS conductance velocities of 16.7 m/s [33]. The regions were interconnected by starting with two single-region networks and then adding synaptic connections between their pyramidal cells while simultaneously lowering the pyramidal-to-pyramidal synaptic connection strength within each region in order to maintain stable delay activity. The following network connection parameters were held constant in the simulations: $G_{\text{pf,if}} = G_{\text{pp,ip}} = 1.02 \text{ mS/cm}^2$; $G_{\text{if,pf}} = G_{\text{ip,pp}} = 1.16 \text{ mS/cm}^2$; $G_{\text{if,if}} = G_{\text{ip,ip}} = 0.65$ (if and ip signify frontal and parietal interneuron populations); $G_{\text{X,if}} = G_{\text{X,ip}} = 0.006 \text{ mS/cm}^2$ (X denotes synapses from the rest of the brain); $G_{\text{X,pf}} = G_{\text{X,pp}} = 0.026 \text{ mS/cm}^2$; $\sigma = 0.2$. In most simulations of the symmetric network, $G_{\text{pf,pf}} = G_{\text{pp,pp}} = 1.21 \text{ mS/cm}^2$, and $G_{\text{pp,pf}} = G_{\text{pf,pp}} = 0.10 \text{ mS/cm}^2$ and $J^+ = 3.2$.

Parameters in the two regions were chosen to be identical to one another, motivated by studies in monkeys, where the activities in areas 8a and 7 were found to be indistinguishable [27, 41], as well as by the similar retinotopy of the intraparietal cortex frontal retinotopy [62]. Recently, this retinotopy has been confirmed in humans with fMRI in both SFS [63] and IPS [64, 65].

The existence of reciprocal SFS–IPS connections has been established in previous studies [66]. In this work, we have made the more specific assumption that there exists a monosynaptic reciprocal connection between the persistently active layer II/III cells in IPS and SFS that we model. Such connections seem to exist from both SFS to IPS [67] and IPS to SFS [62].

Even though the conclusions of this study do not hinge on the exact values of the intra- and inter-regional connection strengths, these values were chosen so that spontaneous and memory activity would be stable both in the presence and absence of the intra-regional connections, as has been seen in vsWM experiments involving cortical cooling (which presumably almost abolishes activity, [41]) in behaving monkeys [41]. This fact imposes an upper bound on the inter-regional connection

strength, because if the combined intra- and inter-regional connection strength is too high or too low, the stability of the spontaneous or mnemonic activity is lost.

A.4. *Simulation protocol*

After an initial transient of 0.5 s during which recordings were discarded, a 3 s inter-trial interval resumed. Thereupon, a 0.5 s, $1 \mu\text{A}/\text{cm}^2$ cue current was introduced into 8% of the pyramidal cells of both modules. A 12 s delay period then followed, and lastly, a 0.5 s, $-3 \mu\text{A}/\text{cm}^2$ current was given to every pyramidal cell in the network to end mnemonic activity. To test network stability, 0.15 s perturbing signals were given simultaneously to both modules at a 180° angle from the cue.

A.5. *Software*

All simulations were performed with the NEURON simulator using the backward Euler algorithm with a time step of 0.02 ms. Model code can be downloaded from NEURON's ModelDB (<http://senselab.med.yale.edu/senselab/modeldb/>). Output from the model was analyzed in MATLAB 6.5.

Acknowledgements

This work was supported by the Foundation for Strategic Research and the Wallenberg Global Learning Network. Fredrik Edin was supported by a PhD Position of Excellence at the Royal Institute of Technology, Stockholm, Sweden. Torkel Klingberg was supported by a research position from the Royal Academy of Sciences through funding from the Knut and Alice Wallenberg foundation. Jesper Tegnér was supported by the Foundation for Strategic Research and the Wennergren foundation. Fredrik Edin, Torkel Klingberg and Jesper Tegnér designed the project. Fredrik Edin implemented the model, ran and analyzed simulations, and preprocessed and analyzed EEG data. Tommy Stödberg collected the EEG data and gave advice on the preprocessing of the EEG data. Fredrik Edin, Torkel Klingberg and Jesper Tegnér wrote the article. We thank Robert Persson for his help with the collection of the EEG data for the DTF analysis, Peter Hedman for working on the preprocessing of the EEG data and Albert Compte for valuable discussions.

References

- [1] Baddeley AD, Hitch GJ, Working memory, *Recent Advances in Learning and Motivation*, pp. 47–49, Academic Press, New York, USA, 1974.
- [2] Engle RW, Tuholski SW, Laughlin JE, Conway AR, Working memory, short-term memory, and general fluid intelligence: A latent-variable approach, *J Exp Psychol Gen* **128**:309–331, 1999.
- [3] Hulme C, Roodenrys S, Practitioner review: Verbal working memory development and its disorders, *J Child Psychol Psychiatry* **36**:373–398, 1995.

- [4] Klingberg T, Limitations in information processing in the human brain: Neuroimaging of dual task performance and working memory tasks, *Prog Brain Res* **126**:95–102, 2000.
- [5] Barkley RA, Behavioral inhibition, sustained attention, and executive functions: Constructing a unifying theory of ADHD, *Psychol Bull* **121**:65–94, 1997.
- [6] Westerberg H, Hirvikoski T, Forssberg H, Klingberg T, Visuo-spatial working memory span: a sensitive measure of cognitive deficits in children with ADHD, *Child Neuropsychol* **10**:155–161, 2004.
- [7] Park S, Holzman PS, Schizophrenics show spatial working memory deficits, *Arch Gen Psychiatry* **49**:975–982, 1992.
- [8] Owen AM, Beksinska M, James M, Leigh PN, Summers BA, Marsden CD, Quinn NP, Sahakian BJ, Robbins TW, Visuospatial memory deficits at different stages of Parkinson's disease, *Neuropsychologia* **31**:627–644, 1993.
- [9] Courtney SM, Petit L, Maisog JM, Ungerleider LG, Haxby JV, An area specialized for spatial working memory in human frontal cortex, *Science* **279**:1347–1351, 1998.
- [10] Klingberg T, Forssberg H, Westerberg H, Increased brain activity in frontal and parietal cortex underlies the development of visuospatial working memory capacity during childhood, *J Cogn Neurosci* **14**:1–10, 2002.
- [11] Curtis CE, Rao VY, D'Esposito M, Maintenance of spatial and motor codes during oculomotor delayed response tasks, *J Neurosci* **24**: 3944–3952, 2004.
- [12] Klingberg T, Development of a superior frontal-intraparietal network for visuo-spatial working memory, *Neuropsychologia* **44**:2171–2177, 2006.
- [13] Olesen PJ, Nagy Z, Westerberg H, Klingberg T, Combined analysis of DTI and fMRI data reveals a joint maturation of white and grey matter in a fronto-parietal network, *Brain Res Cogn Brain Res* **18**:48–57, 2003.
- [14] Edin F, Macoveanu J, Olesen PJ, Tegnér J, Klingberg T, Stronger synaptic connectivity as a mechanism behind development of working memory-related brain activity during childhood, *J Cogn Neurosci* **19**:750–760, 2007.
- [15] Sakai K, Rowe JB, Passingham RE, Active maintenance in prefrontal area 46 creates distractor-resistant memory, *Nat Neurosci* **5**:479–484, 2002.
- [16] Babiloni C, Babiloni F, Carducci F, Cincotti F, Vecchio F, Cola B, Rossi S, Miniussi C, Rossini PM, Functional frontoparietal connectivity during short-term memory as revealed by high-resolution EEG coherence analysis, *Behav Neurosci* **118**:687–697, 2004.
- [17] Kamiński MJ, Blinowska KJ, A new method of the description of the information flow in the brain structures, *Biol Cybern* **65**:203–210, 1991.
- [18] Kamiński M, Ding M, Truccolo WA, Bressler SL, Evaluating causal relations in neural systems: granger causality, directed transfer function and statistical assessment of significance, *Biol Cybern* **85**:145–157, 2001.
- [19] Sharott A, Magill PJ, Bolam JP, Brown P, Directional analysis of coherent oscillatory field potentials in the cerebral cortex and basal ganglia of the rat, *J Physiol* **562**:951–963, 2005.
- [20] Liang H, Ding M, Nakamura R, Bressler SL, Causal influences in primate cerebral cortex during visual pattern discrimination, *Neuroreport* **11**:2875–2880, 2000.
- [21] Ginter J, Jr., Blinowska KJ, Kaminski M, Durka PJ, Pfurtscheller G, Neuper C, Propagation of EEG activity in the beta and gamma band during movement imagery in humans, *Methods Inf Med* **44**:106–113, 2005.

- [22] de Fockert JW, Rees G, Frith CD, Lavie N, The role of working memory in visual selective attention, *Science* **291**:1803–1806, 2001.
- [23] Horwitz B, Tagamets MA, McIntosh AR, Neural modeling, functional brain imaging, and cognition, *Trends Cogn Sci* **3**:91–98, 1999.
- [24] Ungerleider LG, Courtney SM, Haxby JV, A neural system for human visual working memory, *Proc Natl Acad Sci USA* **95**:883–890, 1998.
- [25] Deco G, Rolls ET, Attention, short-term memory, and action selection: A unifying theory, *Prog Neurobiol* **76**:236–256, 2005.
- [26] Kandel ER, Schwarz JH, Jessel TM, *Principles of Neural Science*. 4 ed., New York, USA, McGraw-Hill, 2000.
- [27] Chafee MV, Goldman-Rakic PS, Matching patterns of activity in primate prefrontal area 8a and parietal area 7ip neurons during a spatial working memory task, *J Neurophysiol* **79**:2919–2940, 1998.
- [28] Barbas H, Connections underlying the synthesis of cognition, memory, and emotion in primate prefrontal cortices, *Brain Res Bull* **52**:319–330, 2000.
- [29] Felleman DJ, Van Essen DC, Distributed hierarchical processing in the primate cerebral cortex, *Cereb Cortex* **1**:1–47, 1991.
- [30] Andersen RA, Asanuma C, Essick G, Siegel RM, Corticocortical connections of anatomically and physiologically defined subdivisions within the inferior parietal lobule, *J Comp Neurol* **296**:65–113, 1990.
- [31] Tegnér J, Compte A, Wang X-J, The dynamical stability of reverberatory neural circuits, *Biol Cybern* **87**:471–481, 2002.
- [32] Chafee MV, Goldman-Rakic PS, Inactivation of parietal and prefrontal cortex reveals interdependence of neural activity during memory-guided saccades, *J Neurophysiol* **83**:1550–1566, 2000.
- [33] Ferraina S, Pare M, Wurtz RH, Comparison of cortico-cortical and cortico-collicular signals for the generation of saccadic eye movements, *J Neurophysiol* **87**:845–858, 2002.
- [34] Constantinidis C, Franowicz MN, Goldman-Rakic PS, Coding specificity in cortical microcircuits: a multiple-electrode analysis of primate prefrontal cortex, *J Neurosci* **21**:3646–3655, 2001.
- [35] Ebersole JS, Pedley, TA, *Current Practice of Clinical Electroencephalography*, Lippincott Williams & Wilkins, Philadelphia, USA, 2002.
- [36] Schneider T, Neumaier A, Algorithm 808: ARfit – a Matlab package for the estimation of parameters and eigenmodes of multivariate autoregressive models, *ACM transactions on mathematical software* **27**:58–65, 2001.
- [37] Klimesch W, EEG alpha and theta oscillations reflect cognitive and memory performance: a review and analysis, *Brain Res Brain Res Rev* **29**:169–195, 1999.
- [38] Bastiaansen MC, Posthuma D, Groot PF, de Geus EJ, Event-related alpha and theta responses in a visuo-spatial working memory task, *Clin Neurophysiol* **113**:1882–1893, 2002.
- [39] Worsley KJ, Friston KJ, Analysis of fMRI time-series revisited — again, *Neuroimage* **2**:173–181, 1995.
- [40] Funahashi S, Bruce CJ, Goldman-Rakic PS, Mnemonic coding of visual space in the monkey’s dorsolateral prefrontal cortex, *J Neurophysiol* **61**:331–349, 1989.

- [41] Howard MW, Rizzuto DS, Caplan JB, Madsen JR, Lisman J, Aschenbrenner-Scheibe R, Schulze-Bonhage A, Kahana MJ, Gamma oscillations correlate with working memory load in humans, *Cereb Cortex* **13**:1369–1374, 2003.
- [42] Lutzenberger W, Ripper B, Busse L, Birbaumer N, Kaiser J, Dynamics of gamma-band activity during an audiospatial working memory task in humans, *J Neurosci* **22**:5630–5638, 2002.
- [43] Tallon-Baudry C, Bertrand O, Peronnet F, Pernier J, Induced gamma-band activity during the delay of a visual short-term memory task in humans, *J Neurosci* **18**:4244–4254, 1998.
- [44] Jensen O, Tesche CD, Frontal theta activity in humans increases with memory load in a working memory task, *Eur J Neurosci* **15**:1395–1399, 2002.
- [45] Jensen O, Idiart MA, Lisman JE, Physiologically realistic formation of autoassociative memory in networks with theta/gamma oscillations: role of fast NMDA channels, *Learn Mem* **3**:243–256, 1996.
- [46] Niessing J, Ebisch B, Schmidt KE, Niessing M, Singer W, Galuske RA, Hemodynamic signals correlate tightly with synchronized gamma oscillations, *Science* **309**:948–951, 2005.
- [47] Mukamel R, Gelbard H, Arieli A, Hasson U, Fried I, Malach R, Coupling between neuronal firing, field potentials, and fMRI in human auditory cortex, *Science* **309**:951–954, 2005.
- [48] Lee L, Friston K, Horwitz B, Large-scale neural models and dynamic causal modelling, *Neuroimage* **30**:1243–1254, 2006.
- [49] Horwitz B, Warner B, Fitzer J, Tagamets MA, Husain FT, Long TW, Investigating the neural basis for functional and effective connectivity. Application to fMRI, *Philos Trans R Soc Lond B Biol Sci* **360**:1093–1108, 2005.
- [50] Halgren E, Boujon C, Clarke J, Wang C, Chauvel P, Rapid distributed fronto-parieto-occipital processing stages during working memory in humans, *Cereb Cortex* **12**:710–728, 2002.
- [51] Rowe JB, Toni I, Josephs O, Frackowiak RS, Passingham RE, The prefrontal cortex: Response selection or maintenance within working memory? *Science* **288**:1656–1660, 2000.
- [52] Todd JJ, Marois R, Capacity limit of visual short-term memory in human posterior parietal cortex, *Nature* **428**:751–754, 2004.
- [53] Brunel N, Persistent activity and the single-cell frequency-current curve in a cortical network model, *Network* **11**:261–280, 2000.
- [54] Macoveanu J, Klingberg T, Tegnér J, Neuronal firing rates account for distractor effects on mnemonic accuracy in a visuo-spatial working memory task, *Biol Cybern* **96**:407–419, 2007.
- [55] Olesen PJ, Macoveanu J, Tegnér J, Klingberg T, Brain activity related to working memory and distraction in children and adults, *Cereb Cortex* **17**:1047–1054, 2007.
- [56] Markram H, Lubke J, Frotscher M, Roth A, Sakmann B, Physiology and anatomy of synaptic connections between thick tufted pyramidal neurones in the developing rat neocortex, *J Physiol* **500**:409–440, 1997.
- [57] McCormick DA, Connors BW, Lighthall JW, Prince DA, Comparative electrophysiology of pyramidal and sparsely spiny stellate neurons of the neocortex, *J Neurophysiol* **54**:782–806, 1985.

- [58] Wang XJ, Synaptic reverberation underlying mnemonic persistent activity, *Trends Neurosci* **24**:455–463, 2001.
- [59] Wang XJ, Buzsaki G, Gamma oscillation by synaptic inhibition in a hippocampal interneuronal network model, *J Neurosci* **16**:6402–6413, 1996.
- [60] Destexhe A, Mainen ZF, Sejnowski TJ, Synthesis of models for excitable membranes, synaptic transmission and neuromodulation using a common kinetic formalism, *J Comput Neurosci* **1**:195–230, 1994.
- [61] Watt AJ, van Rossum MC, MacLeod KM, Nelson SB, Turrigiano GG, Activity coregulates quantal AMPA and NMDA currents at neocortical synapses, *Neuron* **26**:659–670, 2000.
- [62] Blatt GJ, Andersen RA, Stoner GR, Visual receptive field organization and cortico-cortical connections of the lateral intraparietal area (area LIP) in the macaque, *J Comp Neurol* **299**:421–445, 1990.
- [63] Kastner S, DeSimone K, Konen CS, Szczepanski SM, Weiner KS, Schneider KA, Topographic maps in human frontal cortex revealed in memory-guided saccade and spatial working-memory tasks, *J Neurophysiol* **97**:3494–3507, 2007.
- [64] Schluppeck D, Glimcher P, Heeger DJ, Topographic organization for delayed saccades in human posterior parietal cortex, *J Neurophysiol* **94**:1372–1384, 2005.
- [65] Silver MA, Ress D, Heeger DJ, Topographic maps of visual spatial attention in human parietal cortex, *J Neurophysiol* **94**:1358–1371, 2005.
- [66] Andersen RA, Asanuma C, Essick G, Siegel RM, Corticocortical connections of anatomically and physiologically defined subdivisions within the inferior parietal lobule, *J Comp Neurol* **296**:65–113, 1990.
- [67] Leichnetz GR, An intrahemispheric columnar projection between two cortical multisensory convergence areas (inferior parietal lobule and prefrontal cortex): an anterograde study in macaque using HRP gel, *Neurosci Lett* **18**:119–124, 1980.